Electronic Supplementary Information

Self-assembly of pyrene derivatives on Au(111): substituent effects on intermolecular interactions

Tuan Anh Pham,*[a] Fei Song,[a] Manh-Thuong Nguyen,[b] Meike Stöhr*[a]

[a] Zernike Institute for Advanced Materials, University of Groningen, Nijenborgh 4, 9747 AG, Groningen, The Netherlands.

[b] The Abdus Salam International Centre for Theoretical Physics, Strada Costiera 11, I-34151 Trieste, Italy.

To whom correspondence should be addressed: t.a.pham@rug.nl; m.a.stohr@rug.nl

Contents

1. Experimental Section

The experiments were carried out in two independent two-chamber ultra-high vacuum systems with a base pressure of 5×10^{-10} mbar. Both systems are equipped with facilities for surface preparation, i.e. Ar^+ ion sputtering and resistive sample heating. The first system houses a variable temperature STM (Oxford Instruments Omicron NanoScience) and a LEED apparatus (SPECS Surface Nano Analysis GmbH). The second system houses a low-temperature STM (Oxford Instruments Omicron NanoScience). The Au(111) single crystal was prepared by repeated cycles of sputtering with Ar^+ ions and annealing at approximately 400°C. Commercially available 1,3,6,8-tetrabromopyrene (Br_4Py) and 2,7-dibromopyrene (Br_2Py) were thoroughly degassed several hours before deposition onto Au(111). The molecules were thermally evaporated from a glass crucible that was heated inside a home-built evaporator. The deposition rate was monitored using a quartz crystal microbalance in order to determine the molecular coverage. The substrate was held at room temperature during deposition. The STM images of Br_4Py/Br_2Py were taken in constant current mode using a platinum-iridium tip at room temperature/77K. The bias voltage is applied to the tip while the sample is grounded. Image processing was done with the free software WSxM.[1]

2. LEED measurements for Br_4Py on Au(111)

LEED measurements were performed to determine the molecular unit cell for the close-packed assembly obtained after deposition of Br_4Py on Au(111) held at room temperature. The LEED pattern was taken for samples held at room temperature (Figure S4). The sample was slightly tilted with respect to normal incidence, allowing the observation the diffraction spots of first order which would be otherwise hidden by the electron gun. The LEED pattern was taken at an energy of 42 eV for the incident electron beam. The software LEEDpat2.1 was used to simulate the experimentally obtained LEED pattern.[2]

3. STM and LEED data

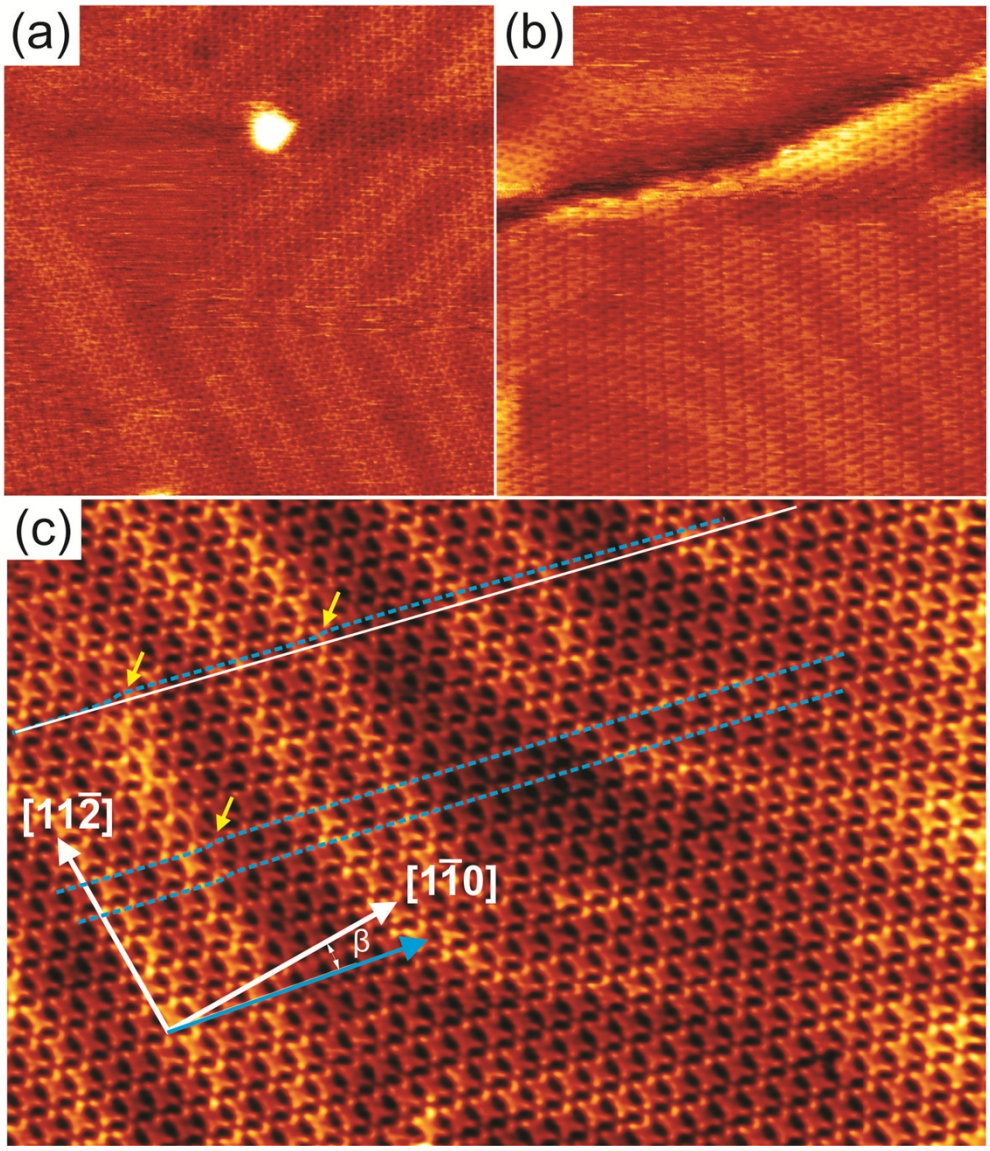

Figure S1. (a) Overview STM image (40×40 nm^2) showing that the herringbone reconstruction is intact under the molecular overlayer. (b) STM image (28×28 nm^2) showing the ordering of the molecules in the vicinity of a step edge. (c) STM image (20×30 nm^2) for 1 ML Br_4Py on Au(111). The principal substrate and molecular adsorption directions are denoted by white and blue arrows, respectively. β is the angle enclosed by the molecular adsorption direction and the [1$\bar{1}$0] substrate direction. The blue dotted lines act as a guide to the eye to indicate the slight shift of the molecular rows with respect to the straight white line. The STM images were taken at room temperature with U = -1.2 V, I = 80 pA.

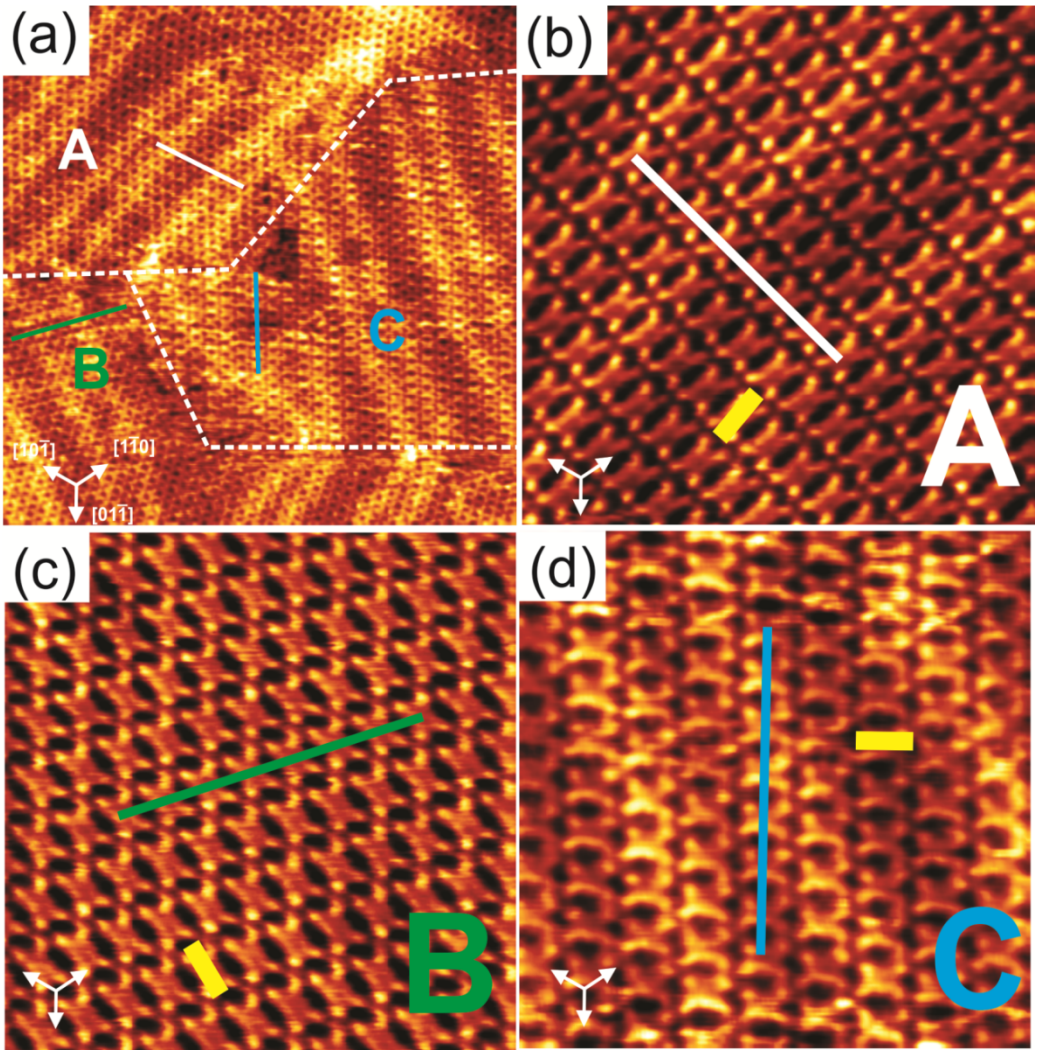

Figure S2. (a) Large scale STM image (38×38 nm^2) of 1ML Br_4Py on Au(111), showing the co-existence of three rotational domains, labeled A, B and C. The white dashed lines mark the domain boundaries. The solid white, green and blue lines in each domain indicate the molecular adsorption direction which is aligned along one of the principal Au directions. (b), (c) and (d) Close-up STM images (10×10 nm^2) of domains A, B and C, respectively. The short yellow line acts as a guide to the eye to indicate the molecular orientation for different domains with respect to the principal Au directions. The STM images were taken at room temperature with U = -1.2 V, I = 60 pA.

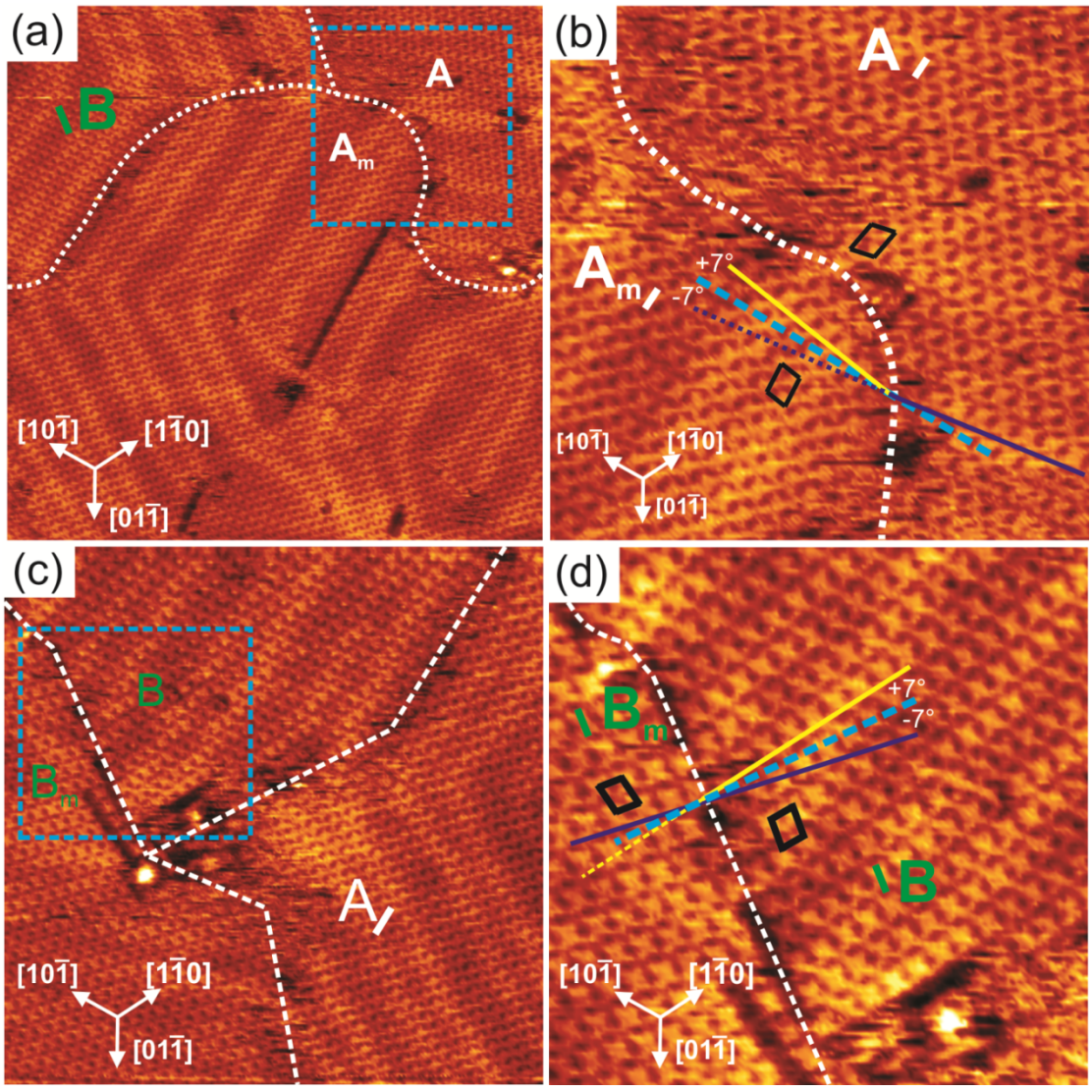

Figure S3. (a) and (c) Overview STM images (50×50 nm^2 and 35×35 nm^2, respectively) of 1 ML Br_4Py on Au(111), showing the co-existence of mirror domains. (b) and (d) Close-up STM images (20×20 nm^2 and 18×18 nm^2, respectively) of the areas marked by blue dotted squares in a) and c), respectively. The domain boundaries are marked by white dashed lines. The unit cells are marked by black rhomboids. The arrangement of the molecules within the unit cell is mirrored at the blue dotted line which is parallel to a principal Au direction. The set of three arrows indicates the principal directions of the substrate. The STM images were taken at room temperature with U = -1.47 V, I = 40 pA.

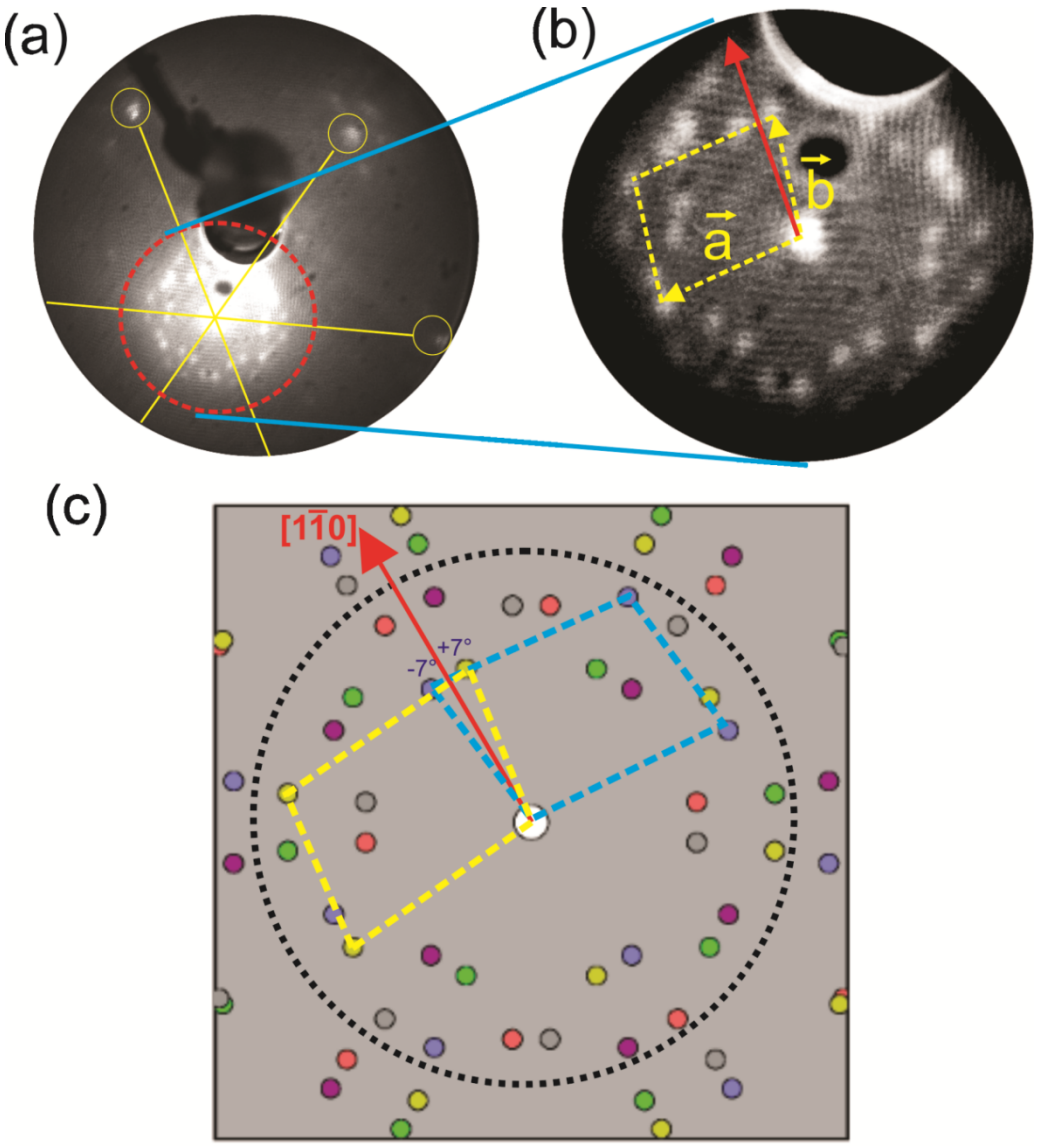

Figure S4. (a) LEED pattern for 1ML Br_4Py on Au(111) taken at a beam energy of 42 eV. The yellow lines act as a guide to the eye to mark the principal directions of the Au(111) substrate. The yellow circles mark the first order spots of the Au(111) substrate. (b) Zoom-in of the area marked by the red dashed circle in a). The unit cell of the molecular adlayer with corresponding vectors $\vec{a}$ and $\vec{b}$ is denoted by the yellow dashed rhomboid. The red arrow indicates one of the principal directions of the substrate. (c) Simulated LEED pattern. The black dashed circle marks

the area where the diffraction spots are visible in b). The yellow and blue dashed rhomboids indicate the unit cells which are mirror images with respect to the principal Au direction. The angle enclosed between the principal Au direction and a unit cell vector amounts to 7° which is in excellent agreement with what is found from the STM analysis (see Figure S3).

The analysis of the LEED pattern yields an incommensurate superstructure for 1 ML of Br_4Py on Au(111) (phase I) . The molecular lattice direction is rotated by an angle of 7º with respect to the principal Au direction. Because the molecular lattice direction does not run parallel to the principal Au direction, it is expected that each of the rotational domains can be mirrored at this substrate direction. Indeed, for each rotational domain a mirror domain can be identified. As a result, the LEED measurements show the co-existence of six domains: three rotational domains multiplied by two because of the existence of mirror domains. The molecular unit cell dimensions determined from LEED are found to be 11.7×8.8 $Å^2$ with an internal angle of 78º, while the ones determined from STM analysis are: a = (11.2 ± 0.2) Å, b = (8.7 ± 0.2) Å, and α = (75 ± 2)°. The findings obtained from the LEED measurements are fully consistent with the STM results for phase I.

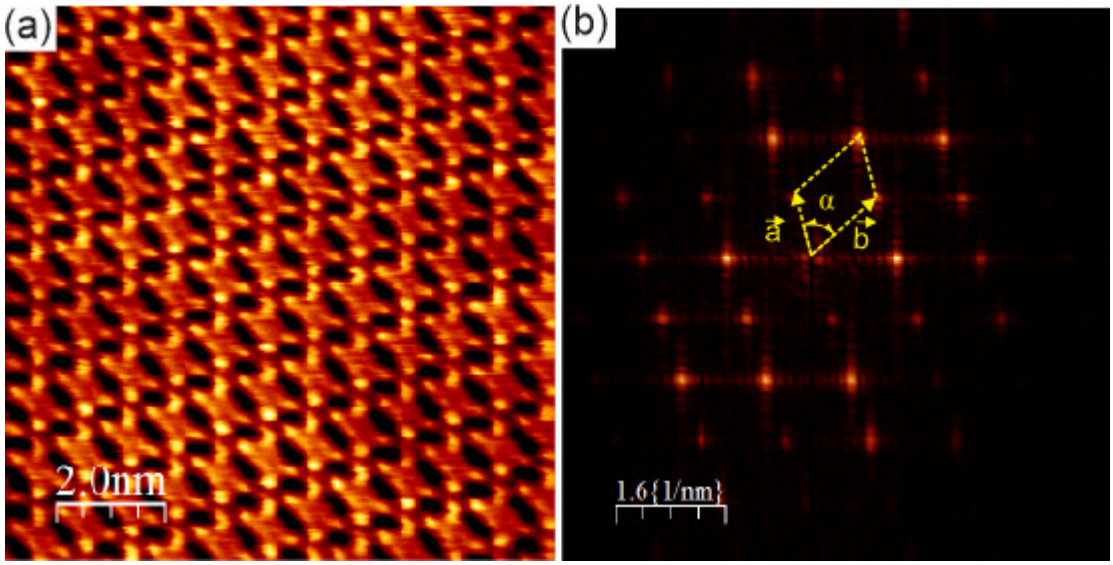

Figure S5. (a) STM image of phase I for Br_4Py on Au(111) and (b) corresponding FFT image.

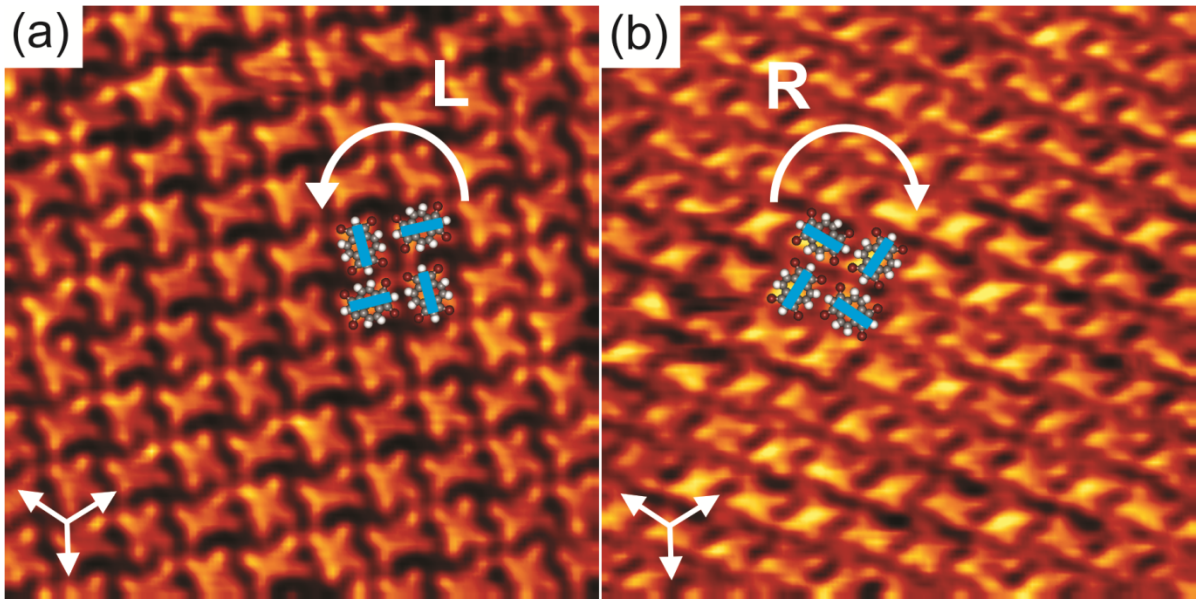

Figure S6. STM images (10×10 nm^2) of the self-assembled pinwheel structure of Br_4Py on Au(111) with (a) anticlockwise and (b) clockwise configuration. The solid blue lines on top of the molecules indicate the molecular orientations within each "pinwheel". The set of three arrows indicates the principal directions of the Au(111) substrate. The STM images were taken at room temperature with U = -1.4 V, I = 40 pA.

4. DFT calculations

Plane-wave density functional theory calculations were carried out using the Quantum ESPRESSO package[3], within the framework of the PBE[4] density functional corrected with semi-empirical dispersion potentials [5] as the van der Waals interactions play a key role in the stability of non-covalently bonded molecules[6]. Additionally, the projector augmented-wave method was employed[7]. We used a kinetic energy cutoff of 40 Ry.

We optimized the geometry of single Br_4Py and Br_2Py in a 22×22×20 $Å^3$ unit cell. Concerning molecular networks, the starting unit cell parameters were chosen from experiments, details are given below. The unit cells were then optimized with the force convergence threshold of 10^{-4} eV/Å. A 2×3×1, 2×2×1, and 2 × 2 × 1 k−point grid was used to sample the Brillouin zone in the self-consistent calculations for phase I, phase II of Br_4Py, and Br_2Py supramolecular nanostructures, respectively. In the geometry optimization processes, the molecules were kept co-planar as they are supposed to be adsorbed on Au(111) in a flat-lying fashion with the same molecule-surface separation. Binding energy per molecule in the molecular networks was calculated as

$$\Delta E = \frac{E_{network} - nE_{single}}{n}$$

where E_{network} is the energy of a unit cell in the network, n (n = 1, 2) is the number of molecules making up the unit cell, and E_{single} is the energy of a single molecule.

The electrostatic potential was calculated as the sum of the potential generated by ions and the Hartree potential.

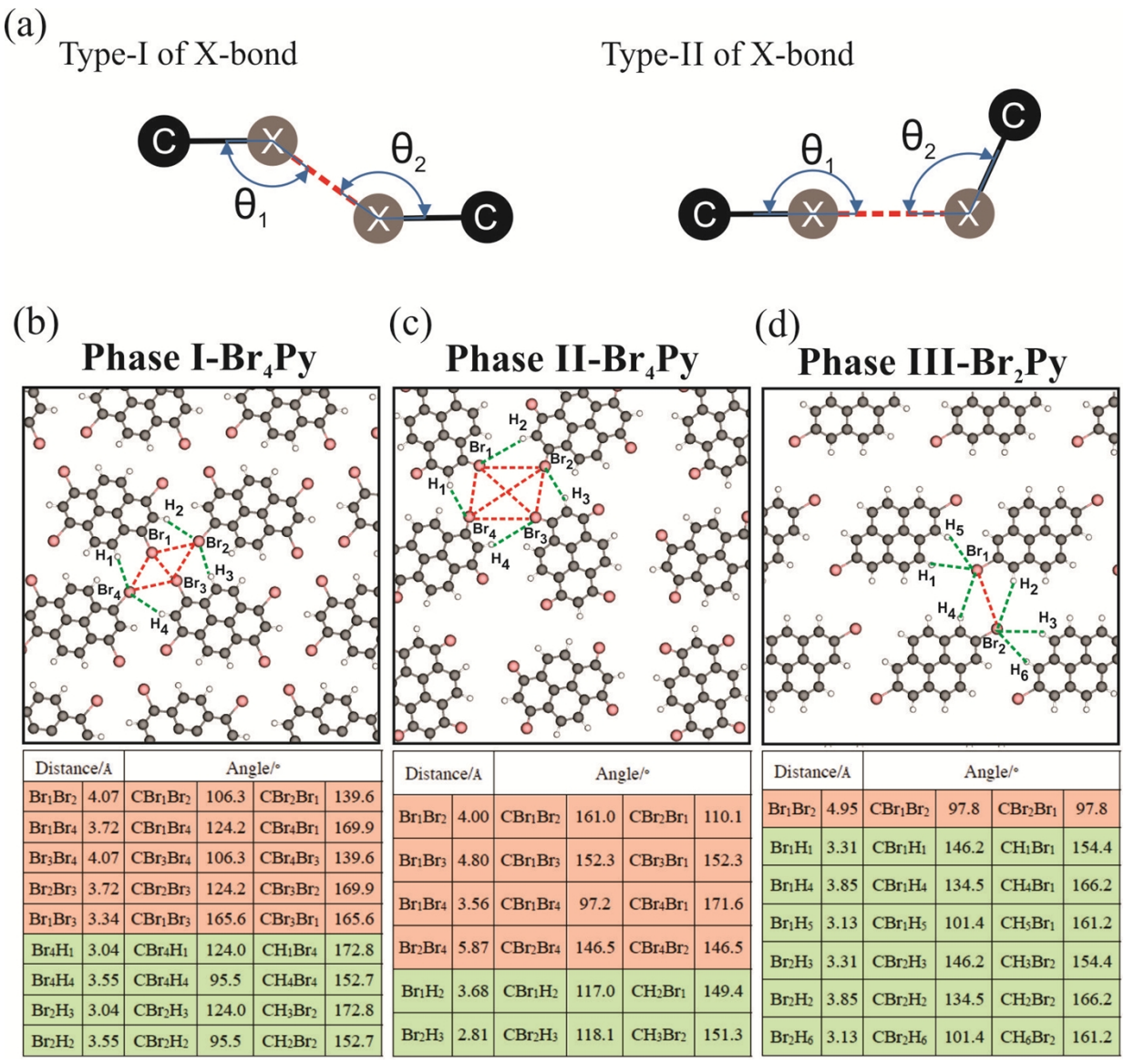

Distance/Å		Angle/°			
Br_1Br_2	4.07	CBr_1Br_2	106.3	CBr_2Br_1	139.6
Br_1Br_4	3.72	CBr_1Br_4	124.2	CBr_4Br_1	169.9
Br_3Br_4	4.07	CBr_3Br_4	106.3	CBr_4Br_3	139.6
Br_2Br_3	3.72	CBr_2Br_3	124.2	CBr_3Br_2	169.9
Br_1Br_3	3.34	CBr_1Br_3	165.6	CBr_3Br_1	165.6
Br_4H_1	3.04	CBr_4H_1	124.0	CH_1Br_4	172.8
Br_4H_4	3.55	CBr_4H_4	95.5	CH_4Br_4	152.7
Br_2H_3	3.04	CBr_2H_3	124.0	CH_3Br_2	172.8
Br_2H_2	3.55	CBr_2H_2	95.5	CH_2Br_2	152.7

Distance/Å		Angle/°			
Br_1Br_2	4.00	CBr_1Br_2	161.0	CBr_2Br_1	110.1
Br_1Br_3	4.80	CBr_1Br_3	152.3	CBr_3Br_1	152.3
Br_1Br_4	3.56	CBr_1Br_4	97.2	CBr_4Br_1	171.6
Br_2Br_4	5.87	CBr_2Br_4	146.5	CBr_4Br_2	146.5
Br_1H_2	3.68	CBr_1H_2	117.0	CH_2Br_1	149.4
Br_2H_3	2.81	CBr_2H_3	118.1	CH_3Br_2	151.3

Distance/Å		Angle/°			
Br_1Br_2	4.95	CBr_1Br_2	97.8	CBr_2Br_1	97.8
Br_1H_1	3.31	CBr_1H_1	146.2	CH_1Br_1	154.4
Br_1H_4	3.85	CBr_1H_4	134.5	CH_4Br_1	166.2
Br_1H_5	3.13	CBr_1H_5	101.4	CH_5Br_1	161.2
Br_2H_3	3.31	CBr_2H_3	146.2	CH_3Br_2	154.4
Br_2H_2	3.85	CBr_2H_2	134.5	CH_2Br_2	166.2
Br_2H_6	3.13	CBr_2H_6	101.4	CH_6Br_2	161.2

Figure S7. (a) Illustration for two different types of X-bonds. (b-d) DFT optimized intermolecular interactions and summarized computed distances and angles for Br-Br and Br-H intermolecular bonds of Br_4Py and Br_2Py molecules.

Depending on the angle between the X-C groups, there are two different types of X-bonds. The type-I X-bond is a repulsive interaction due the similar charge areas of the Br atoms pointing toward each other. This type occurs when $\theta_1 \approx \theta_2$ and their values fall in the range of 140° to

180^{o}. Type-II X-bond is an attractive interaction between the positive and negative charge areas of the halogen atoms. This type occurs when the value of θ_1 falls in the range of 150^{o} to 180^{o} while that of θ_2 falls in the range of 90^{o} to 120^{o}.[8–11] The Br to Br distance for the formation of non-covalent bonds lies in the range of 3.4 to 3.9 Å.[12] For the formation of Br-H hydrogen bonds: if the Br to H distances are larger than 3.5 Å, this hydrogen bond is weak.[13] Then, it was not taken into account. In our case, the computed angles and distances between Br and H atoms fall in the range which is in good agreement with these values. These results confirmed the formation of Br-Br and Br-H bonds in triangular binding motifs which are responsible for the network formation.

(a)

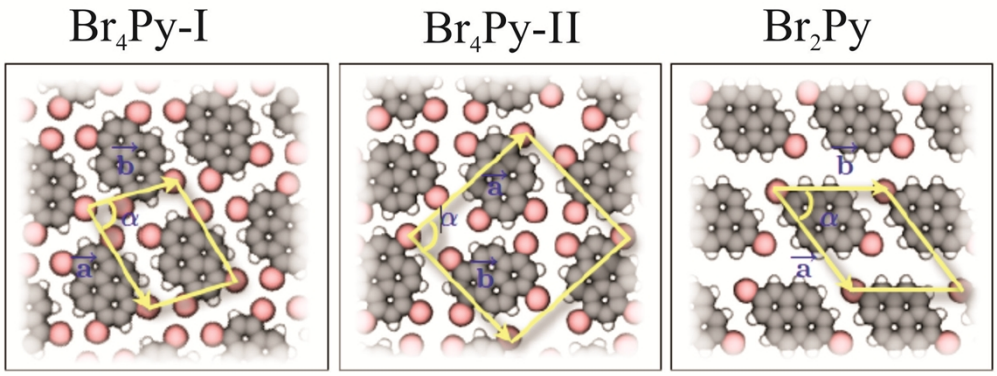

(b)

	Br_4Py-I	Br_4Py-II	Br_2Py
$\lvert\vec{a_e}\rvert$ (Å)	11.2	15.6	11
$\lvert\vec{b_e}\rvert$ (Å)	8.7	14.4	12.7
α_e(°)	73	87	52
$\lvert\vec{a_0}\rvert$ (Å)	11.7	15.4	10.8
$\lvert\vec{b_0}\rvert$ (Å)	9.1	14.3	12.5
α_0(°)	75	87	52
$\lvert\vec{a_1}\rvert$ (Å)	11.7		
$\lvert\vec{b_1}\rvert$ (Å)	8.8		
α_1(°)	78		
ΔE (eV)	0.3	0.28	0.21

Figure S8. (a) DFT optimized unit cell and (b) corresponding geometric and energetic properties for different molecular networks of Br_4Py and Br_2Py. Subscripts e, 1 and 0 in (b) imply the experimentally obtained values from STM, LEED and the computed values, respectively.

5. References

1) I. Horcas, R. Fernández, J.M. Gómez-Rodríguez, J. Colchero, J. Gómez-Herrero, A.M. Baro. *Rev. Sci. Intrum*. 2007, **78**, 013705.
2) http://www.fhi-berlin.mpg.de/KHsoftware/LEEDpat/
3) P. Giannozzi, S. Baroni, N. Bonini, M. Calandra, R. Car, C. Cavazzoni, D. Ceresoli, G. L. Chiarotti, M. Cococcioni, I. Dabo, A. Dal Corso, S. de Gironcoli, S. Fabris, G. Fratesi, R. Gebauer, U. Gerstmann, C. Gougoussis, A. Kokalj, M. Lazzeri, L. Martin-Samos, N. Marzari, F. Mauri, R. Maz- zarello, S. Paolini, A. Pasquarello, L. Paulatto, C. Sbraccia, S. Scandolo, G. Sclauzero, A. P. Seitsonen, A. Smogunov, P. Umari, and R. M. Wentzcovitch, *J. Phys.:Condens. Matter*. 2009, **21**, 395502.
4) J. P. Perdew, K. Burke, and M. Ernzerhof, *Phys. Rev. Lett*. 1996, **77**, 3865.
5) S. Grimme, *J. Comp. Chem*. 2006, **27**, 1787.
6) K. E. Riley and P. Hobza, *Phys. Chem. Chem. Phys*. 2013, **15**, 17742.
7) G. Kresse and D. Joubert, *Phys. Rev. B*., 1999, **59**, 1758.
8) B.K. Saha, R.K.R. Jetti, S. Reddy, S. Aitipamula and A. Nangia, *Cryst. Growth Des*. 2005, **5**, 887.
9) N. Ramasubbu, R. Parthasarathy and P. Murray-Rust. *J. Am. Chem. Soc*. 1986, **108**, 4308.
10) F. Silly, *J. Phys. Chem. C*., 2013, **117**, 20244.
11) J.K. Yoon, W.J. Son, K.H. Chung, H. Kim, S. Han and S.J. Kahng, *J. Phys. Chem. C*., 2011, **115**, 2297.
12) R. Gutzler, O. Ivasenko, C. Fu, J.L. Brusso, F. Roise and D.F. Perepichka, *Chem. Commun*., 2011, **47**, 9455.
13) P.M. Pihko. *Hydrogen Bonding in Organic Synthesis*. Willey-VCH Verlag GmbH & Co. KGaA, Weinheim, 2009.